

# Inter-model variability of projected sea level changes in the western North Pacific in CMIP3 coupled climate models

Masakazu Sueyoshi · Tamaki Yasuda

Received: 2 March 2012 / Revised: 7 May 2012 / Accepted: 8 May 2012 / Published online: 26 May 2012  
© The Oceanographic Society of Japan and Springer 2012

**Abstract** We investigate sea level changes in the western North Pacific for twenty-first century climate projections by analyzing the output from 15 coupled models participating in the Coupled Model Intercomparison Project phase 3 (CMIP3). Projected changes in the wind stress due to those in sea level pressure (SLP) result in the projected sea level changes. In the western North Pacific (30–50°N, 145–170°E), the inter-model standard deviation of the sea level change relative to the global mean is comparable to that based on the multi-model ensemble (MME) mean. Whereas a positive SLP change in the eastern North Pacific (40–50°N, 170–150°W) induces a large northward shift of the Kuroshio Extension (KE), a negative SLP change in this region induces a strong intensification of the KE. Large inter-model variability of the SLP projection in the eastern North Pacific causes a large uncertainty of the sea level projection in the western North Pacific. Models with a larger northward shift (intensification) of the KE exhibit a poleward shift (an intensification) of the Aleutian Low (AL) larger than that for the MME mean. However, models that exhibit a larger intensification of the AL do not necessarily show a larger intensification of the KE. Our analysis suggests that the SLP change that induces an intensification of the KE is associated with a teleconnection from the equatorial Pacific, and that the SLP change that induces a northward shift of the KE is characterized by a zonal mean change.

**Keywords** Sea level · Western North Pacific · Climate change projections · Kuroshio Extension · Aleutian Low

---

M. Sueyoshi · T. Yasuda (✉)  
Climate Research Department, Meteorological Research  
Institute, 1-1 Nagamine, Tsukuba, Ibaraki 305-0052, Japan  
e-mail: tyasuda@mri-jma.go.jp

## 1 Introduction

Coupled climate models used in the Intergovernmental Panel on Climate Change's (IPCC) Fourth Assessment Report (AR4) predict rises in global mean sea level associated with increasing concentrations of atmospheric greenhouse gases (GHGs) (Meehl et al. 2007b). In addition, the models project spatial variations of sea level rise in the twenty-first century (Pardaens et al. 2011; Yin et al. 2010; Slangen et al. 2011).

One of the causes of spatial variations of sea level rise is the change in ocean circulation, especially in the region of a western boundary current such as the Kuroshio Extension (KE) in the North Pacific. Sakamoto et al. (2005) and Sato et al. (2006) showed that sea level in the western North Pacific (30–50°N, 145–170°E) changes in association with increasing greenhouse gas (GHG) forcing. Whereas Sakamoto et al. (2005) found that the KE is intensified in MIROC3.2(hires), Sato et al. (2006) found that the KE shifts northward in MRI-CGCM2.3.2. The difference in the KE changes results from that in the wind stress changes associated with sea level pressure (SLP) changes in the North Pacific. Suzuki et al. (2005) compared sea level projections between MIROC3.2(hires) and a coarse resolution version of it (MIROC3.2(medres)), and also found different sea level change patterns in the western North Pacific between them.

On the basis of the simulations of more than 10 IPCC AR4 coupled models, Meehl et al. (2007b), Pardaens et al. (2011), and Yin et al. (2010) showed that in the KE region the projected increase in the multi-model ensemble (MME) mean sea level is comparable to the inter-model standard deviation of sea level change in the twenty-first century. Yin et al. (2010) used one of the models to show that wind stress changes result in sea

level changes. Suzuki and Ishii (2011) decomposed projected baroclinic sea level changes into vertical modes in MIROC3.2(hires) and found that the changes in the first baroclinic mode are related to pycnocline displacement due to projected wind stress change. In the North Pacific, however, projected SLP and related wind stress changes due to increased GHG forcing differ among IPCC AR4 coupled models (Hori and Ueda 2006; Yamaguchi and Noda 2006; Oshima et al. 2012). Oshima et al. (2012) compared projected SLP changes associated with increased GHGs in 24 IPCC AR4 models and performed a composite analysis in terms of changes in the North Pacific Index (NPI, SLP averaged over 30–65°N and 160°E–160°W, Trenberth and Hurrell 1994). They showed that the spatial pattern of changes in SST in the North Pacific and longitudinally averaged sea level over the North Pacific differ between the case of positive and negative NPI change. This result suggests that in the North Pacific, differences in SLP projections among the models contribute to uncertainty in sea level projections. In order to project sea level change reliably it is therefore necessary to examine whether there is a relationship between model-to-model differences in sea level changes and SLP (wind stress) changes.

In this study we investigate model-to-model differences in projected sea level changes in the western North Pacific and SLP (wind stress) changes in the North Pacific using output from 15 coupled models participating in the Coupled Model Intercomparison Project phase 3 (CMIP3) (Meehl et al. 2007a). We focus on the relationship between inter-model variability of sea level changes associated with changes in the KE and SLP changes. We especially analyze SLP changes that contribute to a northward shift (an intensification) of the KE.

This paper is organized as follows. Section 2 describes the data used in this study. Section 3 presents the results. In Sect. 4, a summary and discussion are described.

## 2 Data

Our analysis is based on the CMIP3 multi-model data set, which is archived by the Program for Climate Model Diagnosis and Intercomparison (PCMDI). Fifteen couple climate models used are listed in Table 1. We use output from the 20th Century Climate in Coupled Models (20C3M) simulation during 1960–1999 and the Special Report on Emission Scenarios (SRES) A1B simulation during 2060–2099 for boreal winter [December–January–February (DJF) average]. The 20C3M simulation is forced with the observed concentration of GHGs. For the A1B simulation, the projection of the greenhouse gas concentration is based on the IPCC SRES A1B emission scenario.

**Table 1** Model names and horizontal resolution of the ocean model (longitude × latitude)

	Name	Resolution
A	CGCM3.1(T47)	1.9° × 1.9°
B	GFDL-CM2.0	1.0° × 1.0°
C	GFDL-CM2.1	1.0° × 1.0°
D	GISS-AOM	4.0° × 3.0°
E	GISS-EH	2.0° × 2.0°
F	GISS-ER	5.0° × 4.0°
G	FGOALS-g1.0	1.0° × 1.0°
H	MIROC3.2(hires)	0.3° × 0.2°
I	MIROC3.2(medres)	1.4° × 1.4°
J	ECHO-G	2.8° × 2.8°
K	ECHAM5	1.5° × 1.5°
L	MRI-CGCM2.3.2	2.5° × 2.0°
M	CCSM3.0	1.1° × 1.0°
N	PCM1	1.1° × 0.7°
O	UKMO-HadCM3	1.3° × 1.3°

For example, the concentration of CO<sub>2</sub> reaches 720 ppm by the year 2100.

In this study, to investigate changes in the regional pattern of sea level, we calculate sea level relative to the global mean. In addition we calculate the global mean steric sea level from temperature and salinity in order to compare this with the magnitude of regional sea level rise. We do not consider the contribution of glaciers, ice caps, and ice sheets to sea level rise. Gregory et al. (2001), Lowe and Gregory (2006), and Landerer et al. (2007) showed that climate models that they used exhibited a drift in the global mean steric sea level in the control run. Therefore it is reasonable to consider that the models in this study exhibit a drift in the global mean steric sea level. It may be impossible to estimate a model drift from the 20C3M simulation because the external forcing is not constant. However, global warming trend is weak in the first half of the twentieth century and therefore we assume the linear trend in the global mean steric sea level during 1901–1930 for the 20C3M,  $T$  (cm/year), to be the model drift. To remove a model drift, 100T is subtracted from the global mean steric sea level change during 2060–2099 relative to 1960–1999. We also estimate the model drift from the linear trend in 1901–1950, but our conclusion is unchanged if these values are used.

To validate model results, we use the sea level anomaly during 1993–2009 obtained from the Archiving, Validation and Interpretation of Satellite Oceanographic (AVISO) data set and the sea level pressure during 1960–1999 obtained from the European Centre for Medium-Range Weather Forecasting 40-year reanalysis data set (ERA40; Uppala et al. 2005).

### 3 Results

#### 3.1 MME mean climatology in the twentieth century

The MME mean climatological sea level relative to the global mean during 1960–1999 is shown in Fig. 1a. Sea level decreases with increasing latitude, and there are strong meridional gradients along 38°N. Here we investigate the impact of wind stress on the distribution of sea level. As a first approximation, the response of the ocean circulation to wind stress can be computed in the following way. Assuming Sverdrup balance (Sverdrup 1947), the vertically integrated velocity can be computed using the wind stress, which is represented by the Sverdrup streamfunction (SSF):

$$\psi(\lambda, \phi) = -\frac{1}{\rho_0\beta} \int_{\lambda}^{\lambda_E} \mathbf{k} \cdot (\nabla \times \boldsymbol{\tau}) R \cos \phi \, d\lambda'. \quad (1)$$

Here  $\lambda$  is the longitude,  $\phi$  is the latitude,  $\lambda_E$  is the longitude of the eastern boundary,  $\rho_0$  ( $=1027 \text{ kg m}^{-3}$ ) is the reference density of sea water,  $\beta$  is the meridional gradient of the Coriolis parameter,  $R$  is the radius of the earth,  $\mathbf{k}$  is the unit vector in the vertical direction, and  $\boldsymbol{\tau}$  is the wind stress vector. We assumed that  $\psi(\lambda_E) = 0$ . The MME mean climatological SSF during 1960–1999 (Fig. 1b) decreases

with increasing latitude, and meridional gradients are large around 38°N. The pattern of sea level is similar to that of the SSF. The sea level distribution is therefore determined largely by the wind stress in the North Pacific. The pattern of the SSF is consistent with that of the wind stress curl; there is a latitude band of negative (positive) wind stress curl south (north) of 40°N (Fig. 1c). The direction of the wind stress is parallel to contours of the SLP due to geostrophy (Fig. 1d). Figure 2 shows the observed climatological SLP during 1960–1999 for DJF based on the ERA40 reanalysis. Apparent in Fig. 2 is a negative SLP anomaly centered at 175°E and 52°N, which is the Aleutian Low (AL). We can see that the models reproduce the AL (Fig. 1d).

The observed climatological sea level relative to the global mean during 1993–2009 based on the AVISO altimetry data (Fig. 3) shows strong meridional gradients in the region east of Japan (KE region). However, with the exception of MIROC3.2(hires), the models fail to reproduce such sharp gradients because the resolution of their ocean models is coarse. Sato et al. (2006) showed that the simulated KE in their ocean model was located north compared to the observed KE. Here we investigate the position and intensity of the KE in the CMIP3 models. We define the latitude of the KE to be the latitude between 34 and 42°N at which the absolute value of the meridional sea

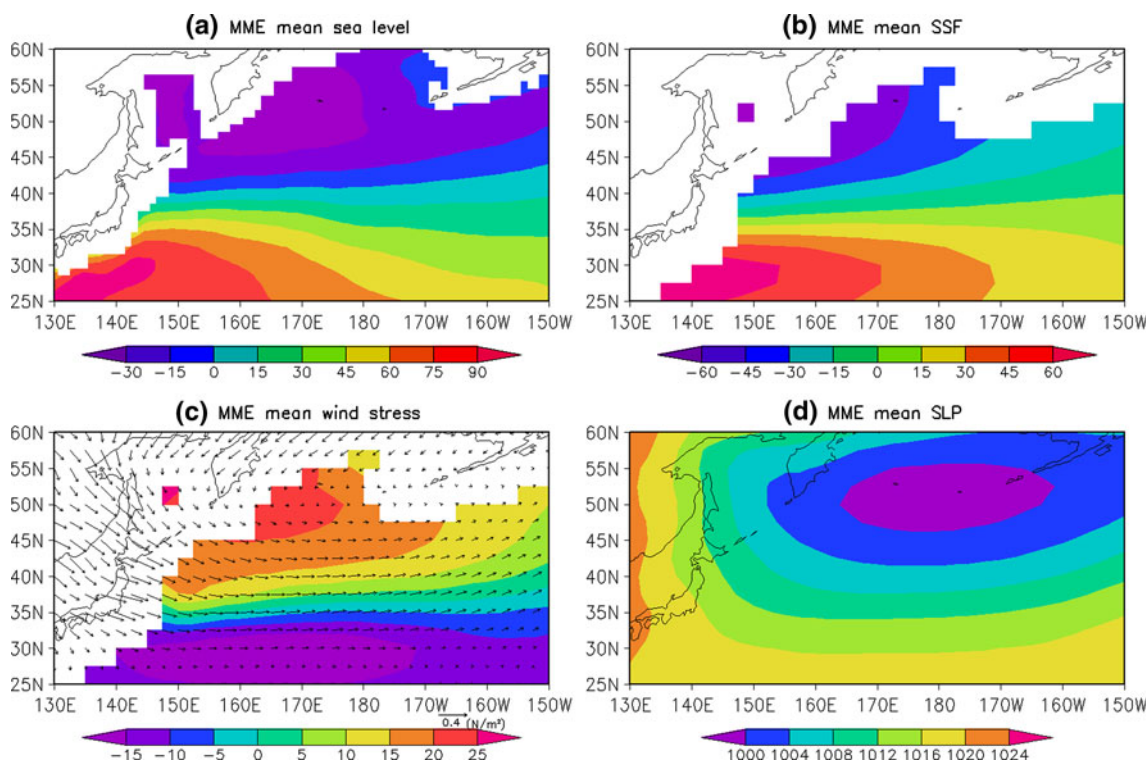


**Fig. 1** MME mean climatological distribution of **a** sea level (cm) relative to the global mean, **b** SSF ( $\text{Sv} = 10^6 \text{ m}^3 \text{ s}^{-1}$ ), **c** wind stress (vector) and its curl ( $10^{-8} \text{ N m}^{-3}$ ), and **d** SLP (hPa) during 1960–1999

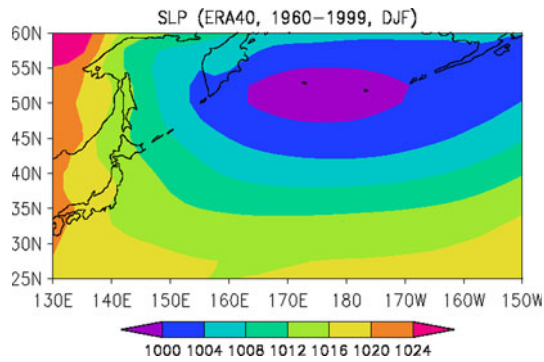


**Fig. 2** Observed climatological SLP (hPa) during 1960–1999 based on the ERA40

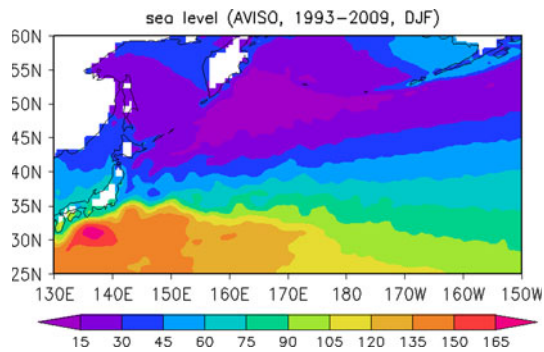


**Fig. 3** Observed climatological sea level (cm) relative to the global mean during 1993–2009 based on the AVISO altimetry data

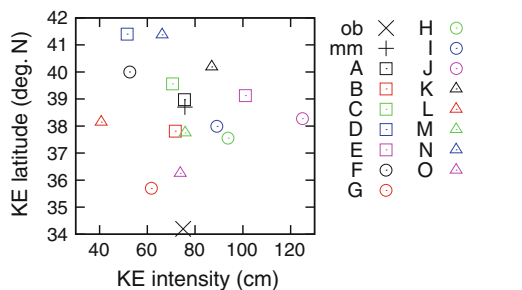


**Fig. 4** Climatological latitude and intensity of the KE during 1960–1999 (the definitions are described in Sect. 3.1). They are averaged values over 150°–165°E. Letters indicate each model (Table 1); *mm* and *ob* indicate the MME mean and observed values based on the AVISO altimetry data, respectively

level gradient is a maximum; the intensity of the KE is defined as the meridional sea level difference between 34 and 42°N (sea level at 34°N minus that at 42°N). In Fig. 4, the climatological intensity of the KE for 1960–1999 is plotted against the climatological latitude of the KE; they are averaged values over 150–165°E. The MME mean intensity of the KE (75.7 cm) is comparable to the observed intensity (75.0 cm). On the other hand, the MME mean latitude of the KE (38.7°N) is larger than the

observed latitude (34.2°N). The KE in all models is located north compared with the observed KE.

### 3.2 Projected changes

The MME mean climatological sea level relative to the global mean during 2060–2099 relative to 1960–1999 is shown in Fig. 5a. The global mean steric sea level rise is not included in Fig. 5a and should be added to obtain the total sea level rise. A positive sea level anomaly between 33 and 40°N extends eastward. On the basis of the MME mean, the global mean steric sea level rise is 15.8 cm (2060–2099 minus 1960–1999), and the increase in the sea level relative to the global mean averaged over the region (30–40°N, 150–165°E) is 8.8 cm (note that the latter does not include the global mean steric sea level rise). The sea level rise relative to the global mean in the region east of Japan is larger than 50 % of the global mean steric sea level rise. The MME mean climatological SSF during 2060–2099 relative to 1960–1999 is shown in Fig. 5b. Sea level and SSF increase in a latitude band centered near 37°N. The wind stress change therefore causes the sea level change. The positive SSF anomaly in the western North Pacific arises from a negative wind stress curl anomaly centered at 37°N extending eastward from the Japan coast (Fig. 5c). An anticyclonic wind stress change south of 40°N is associated with a positive SLP anomaly (Fig. 5d). Consequently, the negative wind stress curl anomaly is associated with this positive SLP anomaly.

It is important to focus on model-to-model differences in sea level change. The inter-model standard deviation of the sea level change (Fig. 6) exceeds 10 cm in a latitude band around 37°N extending eastward from the Japan coast to 175°E. In this band the inter-model standard deviation is comparable to the MME mean increase in sea level (Fig. 5a). A comparison of the global mean steric sea level rise and the average increase in sea level (relative to the global mean) over the region (30–40°N, 150–165°E) in each model (Fig. 7) reveals that in nine models, the average increase is larger than 50 % of the global mean steric sea level rise. Ocean circulation changes due to wind stress change therefore make an important contribution to regional sea level changes.

### 3.3 Composite analysis based on projected change in the KE

In Fig. 8, the future change in the intensity of the KE is plotted against that in the latitude of the KE averaged over 150–165°E. Four models (C, E, I, and L) show a larger northward shift of the KE, and four models (B, D, H, and K) show a stronger intensification of the KE. We perform a composite analysis based on these models. The composite

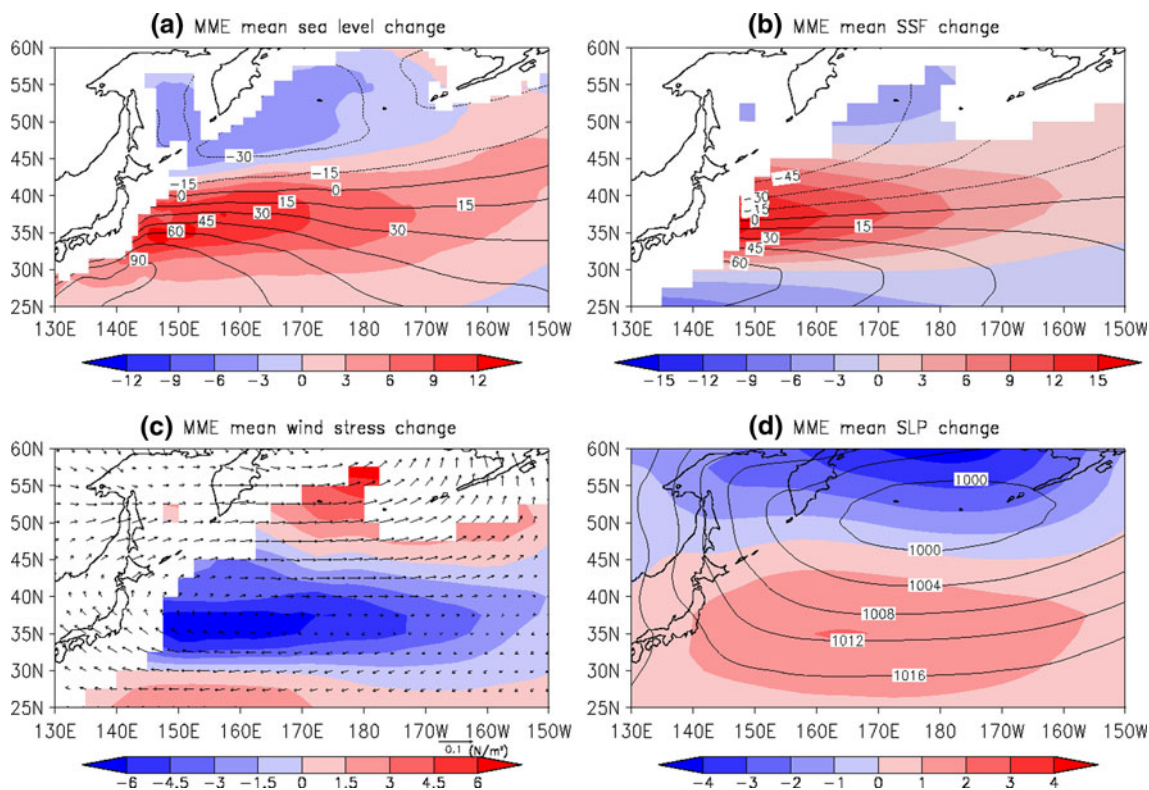


**Fig. 5** MME mean climatological distribution of **a** sea level (cm) relative to the global mean, **b** SSF (Sv), **c** wind stress (vector) and its curl ( $10^{-8} \text{ N m}^{-3}$ ), and **d** SLP (hPa) during 2060–2099 relative to

1960–1999 (shading). The global mean steric sea level rise is not included in **a** and should be added to obtain the total sea level rise. Contours show the distribution during 1960–1999

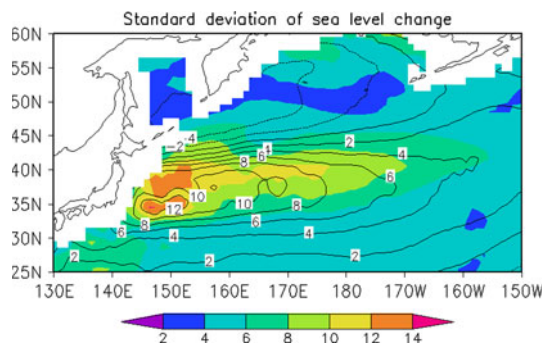


**Fig. 6** Inter-model standard deviation (shading) of the sea level change (cm) (2060–2099 minus 1960–1999). Contours show the MME mean sea level change with the global mean subtracted

sea level distributions relative to the global mean during 2060–2099 relative to 1960–1999 for the four models which have a larger northward shift and a stronger intensification of the KE are shown in Fig. 9a and b, respectively. Note that the global mean steric sea level rise is not included in Fig. 9a and b. In the case of a northward shift, the sea level change pattern shows a positive anomaly centered near the present-day KE. In the case of an intensification, the pattern exhibits a north–south dipole, with positive changes to the south. This positive anomaly is

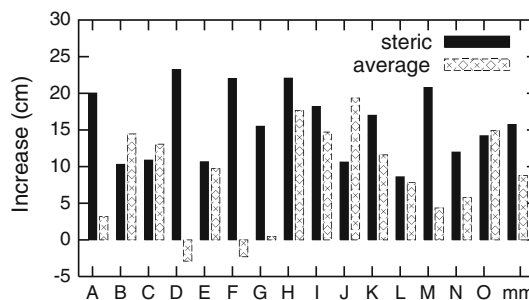


**Fig. 7** Global mean steric sea level rise (black) and increase in the sea level (relative to the global mean) averaged over the region (30–40°N, 150–165°E) (white) for each model (2060–2099 minus 1960–1999). mm indicates the MME mean. Note that the values indicated by white bars do not include the global mean steric sea level rise. We remove the drift in the global mean steric sea level rise (the method is described in Sect. 2)

located south of the KE. In each case the pattern of the composite SSF change (Fig. 9c, d) resembles that of the composite sea level change. The different wind stress changes can therefore explain the differences between sea level (KE) changes. In the models with a northward shift, a negative wind stress curl anomaly is centered at 37°N and 180° (Fig. 9e). In contrast, in the models with an intensification, a negative wind stress curl anomaly centered at

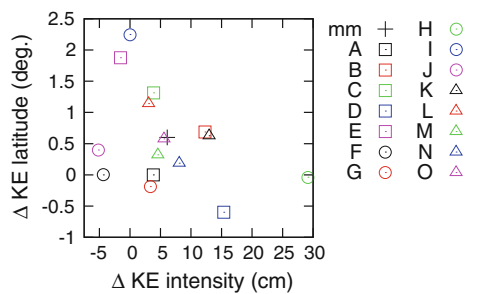


**Fig. 8** Change in the latitude and intensity of the KE (2060–2099 minus 1960–1999). They are averaged values over 150–165°E. Letters and *mm* indicate each model (Table 1) and the MME mean change, respectively

35°N extends eastward from the Japan coast, and a positive anomaly is located around 55–60°N (Fig. 9f). As shown in Fig. 5c and d, the negative (positive) wind stress curl anomalies are associated with positive (negative) SLP anomalies (Fig. 9g, h). In the eastern North Pacific near 45°N and 170°W, the models with a northward shift (intensification) exhibit a positive (negative) SLP change. The difference of the composite SLP change between the northward shift and the intensification of the KE (i.e., Fig. 9g, h) has a maximum near 45°N and 165°W (Fig. 10a). The SLP change in the eastern North Pacific (40–50°N, 170–150°W) is therefore linked to the change in the KE, which induces a sea level change in the KE region. The inter-model standard deviation of the SLP change based on the 15 models has a maximum in the eastern North Pacific (Fig. 10b). In this region the inter-model standard deviation of the SLP change is larger than the magnitude of the MME mean change. Similar results were obtained by Oshima et al. (2012). The results in this section indicate that SLP projections in the eastern North Pacific are important for sea level projections in the western North Pacific.

#### 3.4 Projected change in the Aleutian Low and its relationship with the KE change

From an analysis of observed data, Sugimoto and Hanawa (2009) showed that there is a relationship between inter-annual variability of the AL and the SSF. A poleward shift of the AL results in a northward shift of the zero SSF line, which indicates the boundary between the subtropical and subpolar gyres, and an intensification of the AL leads to an increase of the eastward transport estimated from the SSF. Previous studies (Hori and Ueda 2006; Yamaguchi and Noda 2006) and the results shown in Fig. 10 suggest that changes in the position and intensity of the AL due to increased GHG forcing differ from model to model. Here we investigate a relationship between future changes in the AL and SSF and their impact on sea level in the KE region.

According to Sugimoto and Hanawa (2009), the position of the AL is defined as the position at which SLP has a minimum in the North Pacific (30–65°N, 160°E–160°W). The change in the latitude of the zero line of the climatological SSF is plotted against that in the latitude of the AL in Fig. 11a. The former is averaged value over 150–165°E. The correlation coefficient between them is 0.79. Models with a larger northward shift of the AL therefore tend to show a larger northward shift of the zero SSF line. The change in the eastward transport between 34 and 42°N estimated from the climatological SSF is plotted against that in the intensity of the AL in Fig. 11b. The correlation coefficient between them is –0.55. Therefore models with a larger intensification of the AL tend to exhibit a larger increase in eastward transport. In the four models with a relatively large northward shift of the KE (models C, E, I, and L), the poleward shift of the AL (+3.9°) is larger than that for the MME mean (+1.5°), and the change in the intensity of the AL (–1.8 hPa) is comparable to that for the MME mean (–1.8 hPa). In contrast, in the four models with a relatively strong intensification of the KE (models B, D, H, and K), the poleward shift of the AL (+2.0°) is slightly larger than that for the MME mean, and the AL is more intensified (–2.8 hPa). SLP changes in the eastern North Pacific cause sea level changes in the western North Pacific, and inter-model differences in the former are related to a northward shift and an intensification of the AL.

In the four models showing a relatively strong intensification of the KE, the AL is intensified (Fig. 11b). In three of these models (B, D, and K), however, the magnitude of the intensification of the AL is comparable to that for the MME mean. In models A, C, E, G, M, and N, the AL is largely intensified compared to that in models B, D, and K, but the KE is less intensified (Fig. 8). Thus, a relatively strong intensification of the AL does not necessarily lead to a relatively strong intensification of the KE. We shall discuss this point later (Sect. 4).

#### 3.5 Atmospheric changes related to a northward shift and an intensification of the KE

In Sect. 3.3 we showed that eastern North Pacific SLP changes, which determine western North Pacific sea level changes, differ among the models. Results from IPCC AR4 coupled models have shown that SLP changes over the North Pacific in response to increased GHG forcing are related to the local Hadley circulation (Hori and Ueda 2006) and SST change in the tropics (Yamaguchi and Noda 2006). Here we investigate atmospheric changes related with a northward shift and an intensification of the KE. Figure 12 shows composite changes in sea surface temperature (SST), precipitation, and streamfunction at

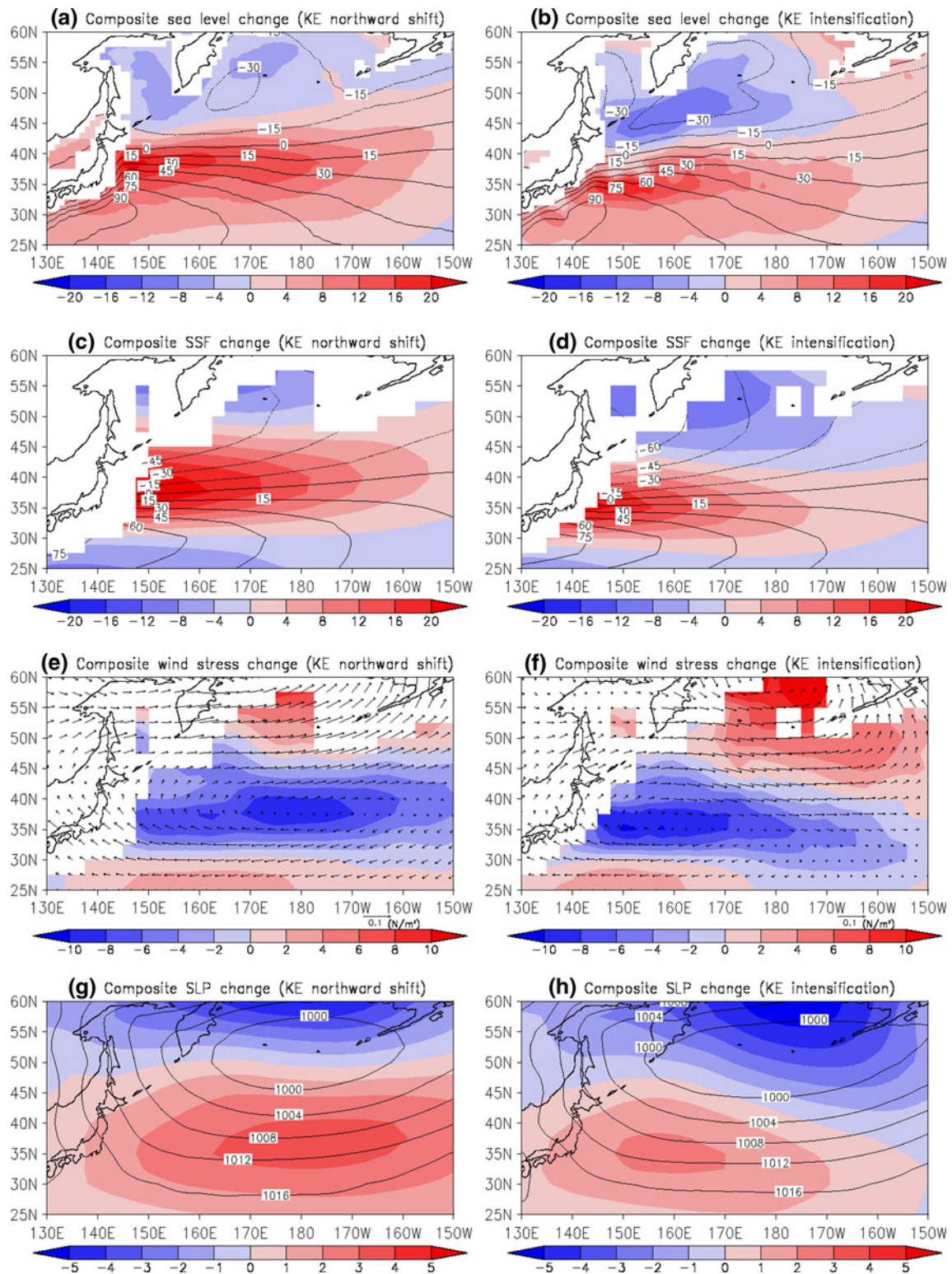


**Fig. 9** Composite climatological distribution of **a** sea level (cm) relative to the global mean, **c** SSF (Sv), **e** wind stress (vector) and its curl ( $10^{-8} \text{ N m}^{-3}$ ), and **g** SLP (hPa) during 2060–2099 relative to 1960–1999 (*shading*) for four models with a relatively large northward shift of the KE (models C, E, I, and L). *Contours* show the composite distribution during 1960–1999. Also shown are the

composite climatological distribution of **b** sea level relative to the global mean, **d** SSF, **f** wind stress (vector) and its curl, and **h** SLP during 2060–2099 relative to 1960–1999 for four models with a relatively strong intensification of the KE (models B, D, H, and K). The global mean steric sea level rise is not included in **a** and **b**

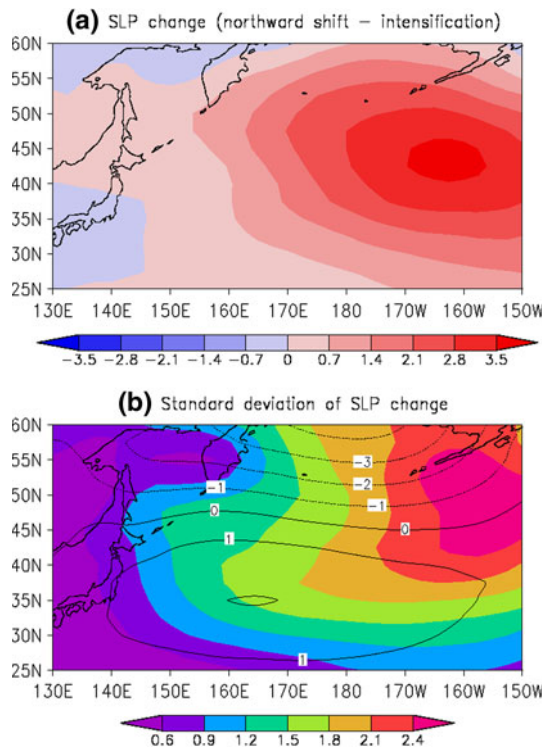


**Fig. 10** **a** Composite difference in the SLP change (hPa) (2060–2099 minus 1960–1999) between four models with a relatively large northward shift of the KE and those with a relatively strong intensification of the KE (the former minus the latter). **b** Inter-model standard deviation of the SLP change based on 15 models (*shading*). *Contours* show the MME mean SLP change

850 hPa for four models with a larger northward shift (a stronger intensification) of the KE. In the case of an intensification of the KE, a strong positive precipitation anomaly is located in the central equatorial Pacific (Fig. 12d). A positive SST change around 180° in the tropics (Fig. 12b) results in this precipitation anomaly. In Fig. 12f, we see a wave train with a negative streamfunction anomaly near 15°N, 150°E, a positive anomaly near 35°N, 160°E, and a negative anomaly near 55°N, 170°W. These results suggest a teleconnection pattern from the equatorial Pacific to the North Pacific. In the North Pacific, the pattern of the streamfunction change in Fig. 12f resembles that of the SLP (wind stress curl) change in the case of an intensification of the KE (Fig. 9f, h). These three fields have a zonal asymmetry around 35–45°N in the North Pacific. For example, at 40°N, the sign of the change at 160°E is opposite to that at 150°W. Our analysis in this section suggests that the negative SLP change in the eastern North Pacific (Fig. 9h) is associated with the teleconnection pattern from the equatorial Pacific in the case of an intensification of the KE.

In the case of a northward shift of the KE (Fig. 12e), a wave train like that in the case of an intensification is not found. In addition, the SST anomaly and precipitation

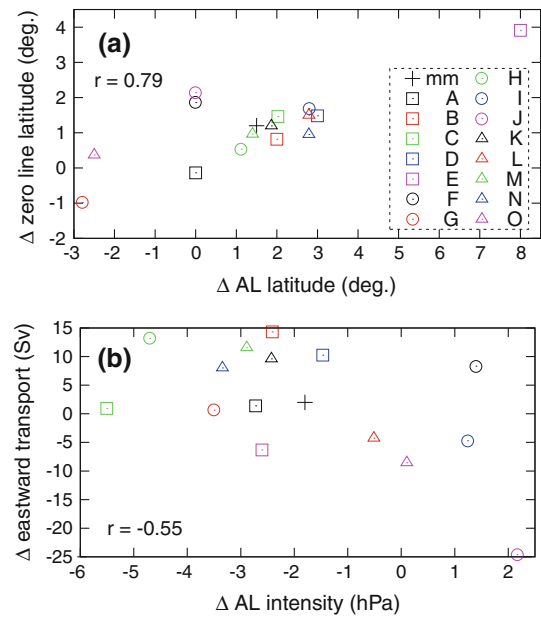


**Fig. 11** **a** Change in the latitude of the zero line of the climatological SSF and in the latitude of the AL (2060–2099 minus 1960–1999). The former is the averaged value over 150–165°E. **b** Change in the eastward volume transport between 34 and 42°N calculated from the climatological SSF versus the change in the intensity of the AL. The former is the averaged value over 150–165°E. *Letters* and *mm* indicate each model (Table 1) and the MME mean change, respectively. Correlation coefficients are shown

anomaly in the central equatorial Pacific around 180° (Fig. 12a, c) are weak compared with those in Fig. 12b and d. Therefore a teleconnection from the equatorial Pacific may be weak in the case of a northward shift. In the North Pacific, the streamfunction change pattern (Fig. 12e) is similar to the pattern of the SLP (wind stress) change (Fig. 9e, g). These three fields are zonally symmetric in the North Pacific. An examination of composite zonal mean SLP changes (Fig. 13) reveals that the increase of the north–south SLP gradient is more apparent in the case of a northward shift than in the case of an intensification. Therefore the SLP change in the North Pacific is characterized by a zonal mean change in the case of a northward shift of the KE.

#### 4 Summary and discussion

We investigated the projected sea level changes in the western North Pacific by using output from the 15 CMIP3 coupled climate models. On the basis of the MME mean, the sea level rise relative to the global mean in the region east of Japan is larger than 50 % of the global mean steric sea level rise. The projected wind stress change determines the projected sea level change in the western North Pacific. In the western North Pacific, the inter-model standard



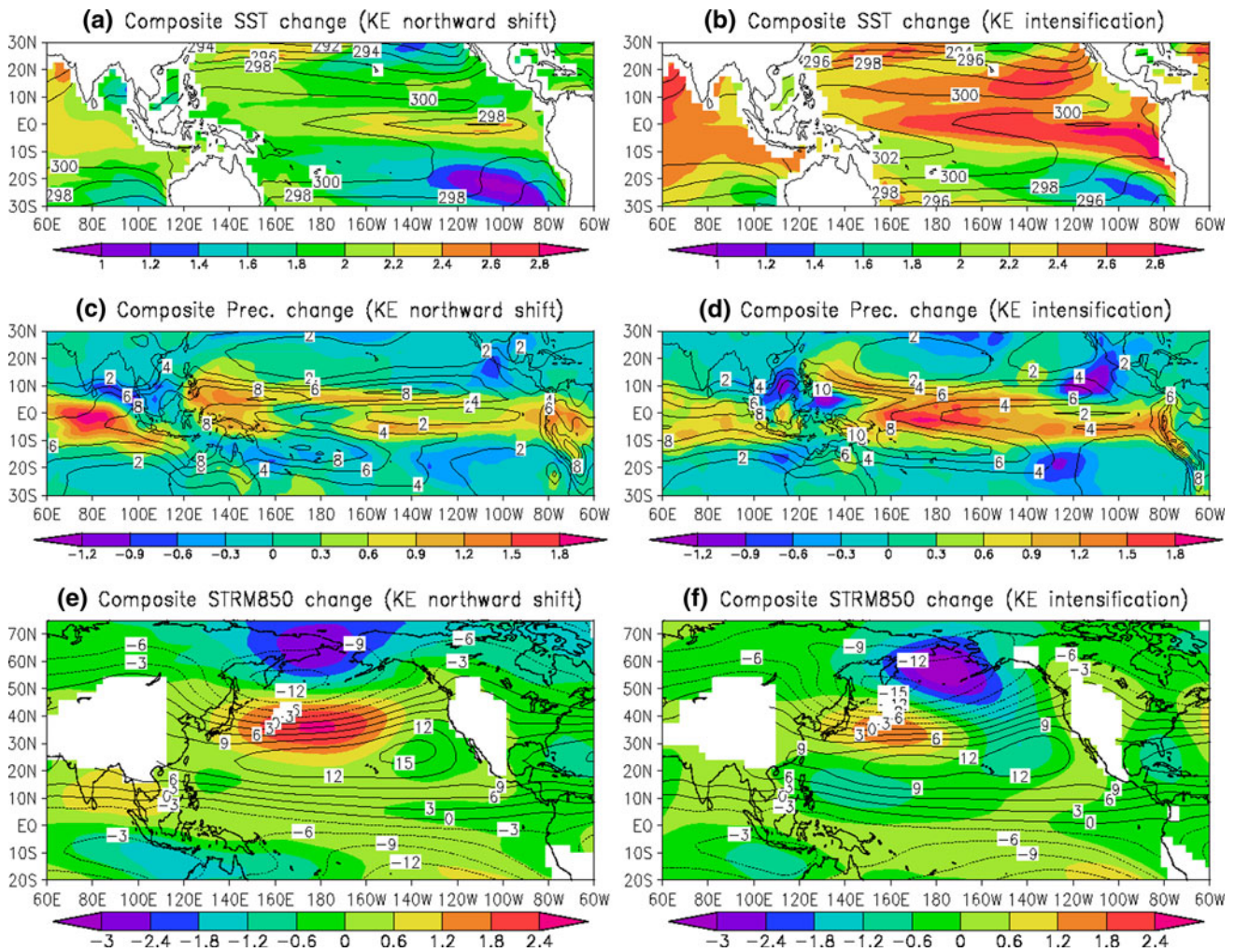


**Fig. 12** Composite climatological distribution of **a** sea surface temperature (K), **c** precipitation (mm day<sup>-1</sup>), and **e** streamfunction (10<sup>6</sup> m<sup>2</sup> s<sup>-1</sup>) at 850 hPa during 2060–2099 relative to 1960–1999 (shading) for four models with a relatively large northward shift of

the KE. *Contours* show the composite distribution during 1960–1999. **b**, **d**, and **f** are the same as **a**, **c**, and **e**, respectively, but for four models with a relatively strong intensification of the KE

deviation of the sea level change relative to the global mean is comparable to that for the MME mean. A northward shift and an intensification of the KE characterize the differences in sea level change in the western North Pacific among the models. A positive (negative) SLP change in the eastern North Pacific induces a northward shift (an intensification) of the KE. In the eastern North Pacific, the inter-model standard deviation of the SLP change based on the 15 models is larger than the magnitude of the MME mean SLP change. Therefore, SLP projections in the eastern North Pacific are important for sea level projections in the western North Pacific.

As we described, a relatively strong intensification of the AL does not necessarily lead to a relatively strong intensification of the KE. Oshima et al. (2012) showed the pattern of composite SLP change in the North Pacific for an intensification of the AL. That pattern is different from the pattern for an intensification of the KE in our study

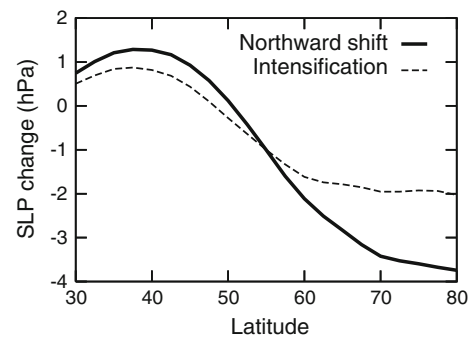


**Fig. 13** Composite climatological distribution of zonal mean SLP change (hPa) during 2060–2099 relative to 1960–1999. *Solid (broken) line* indicates that for four models with a relatively large northward shift (strong intensification) of the KE

(Fig. 9h). In the case of an intensification of the KE, the SLP decreases around the center of the AL and increases in the subtropical gyre region, as shown in Fig. 9h. In

contrast, Oshima et al. (2012) showed that the SLP change is small in the subtropical gyre region in the case of an intensification of the AL. Such a small SLP change leads to a small SSF change in the subtropical gyre region because the SSF change is proportional to the longitudinal integration of the wind stress curl change (note that a wind stress curl anomaly is associated with an SLP anomaly). As a result, there is little intensification of the KE.

In the twentieth century the KE in the 15 models is located north compared with observed KE (Fig. 4). In general the KE simulated in a coarse resolution ocean model is broad meridionally and is located further north than the observed KE position (Sato et al. 2006). Sato et al. (2006) conducted a simulation with a high resolution ocean model ( $1/4^\circ \times 1/6^\circ$ ) forced by atmospheric fields in the future climate projected by MRI-CGCM2.3.2, which has a coarse resolution ocean model. In both models large sea level rises occur in a latitudinal band of large SSF increase around  $35\text{--}40^\circ\text{N}$  in the western North Pacific (note that the SSFs are the same in both models). Thus, the effect of the wind stress on ocean currents in the coarse resolution models that we investigated in this paper is qualitatively applicable to ocean currents in a higher resolution model. The magnitudes of projected sea level change in a model, however, may be influenced by the resolution of the ocean model. In fact, MIROC3.2(hires), whose resolution of the ocean model is highest among the CMIP3 coupled models, shows the largest amplitude of sea level change related to the KE intensification in a future climate. In order to discuss the projection of sea level in this region more quantitatively, many coupled models with higher resolution are needed. Furthermore, it has been suspected that in coarse resolution coupled models the atmospheric fields in the North Pacific are biased because of insufficient reproducibility of the KE (Sakamoto et al. 2005; Kwon et al. 2010). The simulated change in the atmosphere associated with increasing GHGs in a coupled model may be influenced by the resolution of the ocean model.

We showed the present-day position and intensity of the KE in the models (Fig. 4). These are a measure of the reproducibility of the sea level field in the KE region because these can be compared with the observed position and intensity of the KE (Fig. 4). We compare these with the future changes in the position and intensity (Fig. 8) and find that there is no relationship between the reproducibility and the future change (not shown). Therefore we do not evaluate a model ranking based on this reproducibility and do not calculate a weighted ensemble of projections based on a model ranking. Instead of doing this, we showed that the KE change is determined by the SLP change in the eastern North Pacific and that changes in the tropical atmosphere and ocean, to some extent, contribute to this

SLP change. To investigate what influences future projection is useful for the study of climate prediction.

Our analysis in Sect. 3.5 suggests that the negative SLP change in the eastern North Pacific is associated with a teleconnection pattern from the equatorial Pacific in the case of an intensification of the KE and that the SLP change in the North Pacific is characterized by a zonal mean change in the atmosphere in the case of a northward shift of the KE. To fully understand the effect of the tropical warming on the SLP change in the North Pacific under global warming conditions in the models, one must answer the following two questions. First, how does the mid-latitude atmosphere respond to the tropical warming associated with increased GHGs in the models? Oshima and Tanimoto (2009) showed that the correlation between the Pacific Decadal Oscillation index and the decadal El Niño-Southern Oscillation (ENSO) index differs among the CMIP3 models. This suggests that the response of the mid-latitude atmosphere to tropical heat sources differs from model to model. Second, are there any atmospheric (oceanic) processes outside the equatorial Pacific influencing the SLP change in the North Pacific that we focused on? The answers to these questions will be the subject of future work.

**Acknowledgments** This work was supported by the Global Environmental Research Fund (S-5-2) of the Ministry of the Environment, Japan. We acknowledge the modeling groups, the Program for Climate Model Diagnosis and Intercomparison (PCMDI) and the WCRP's Working Group on Coupled Modelling (WGCM), for their roles in making available the WCRP CMIP3 multi-model data set. Support for this data set is provided by the Office of Science, U.S. Department of Energy. We are thankful for the altimeter products produced by Ssalto/Duacs and distributed by AVISO with support from the Centre National d'études Spatiales (CNES). We thank Kazuhiro Oshima, Youichi Tanimoto, and Tomoaki Ose for their useful comments. We are also grateful to Osamu Arakawa for archiving data. We thank two anonymous reviewers for their suggestions, which were useful for improving the manuscript.

## References

- Gregory JM, Church JA, Boer GJ, Dixon KW, Flato GM, Jackett DR, Lowe JA, O'Farrell SP, Roeckner E, Russell GL, Stouffer RJ, Winton M (2001) Comparison of results from several AOGCMs for global and regional sea-level change 1900–2100. *Clim Dyn* 18:225–240
- Hori ME, Ueda H (2006) Impact of global warming on the East Asian winter monsoon as revealed by nine coupled atmosphere-ocean GCMs. *Geophys Res Lett* 33(L03713). doi:10.1029/2005GL024961
- Kwon YO, Alexander MA, Bond NA, Frankignoul C, Nakamura H, Qiu B, Thompson LA (2010) Role of the Gulf Stream and Kuroshio–Oyashio systems in large-scale atmosphere–ocean interaction: a review. *J Clim* 23:3249–3281. doi:10.1175/2010JCLI3343.1
- Landerer FW, Jungclaus JH, Marotzke J (2007) Regional dynamic and steric sea level change in response to the IPCC-A1B scenario. *J Phys Oceanogr* 37:296–312

- Lowe JA, Gregory M (2006) Understanding projections of sea level rise in a Hadley Centre coupled climate model. *J Geophys Res* 111(C11014). doi:[10.1029/2005JC003421](https://doi.org/10.1029/2005JC003421)
- Meehl GA, Covey C, Delworth T, Latif M, McAvaney B, Mitchell JFB, Stouffer RJ, Taylor KE (2007a) The WCRP CMIP3 multi-model dataset: a new era in climate change research. *Bull Am Meteorol Soc* 88:1383–1394. doi:[10.1175/BAMS-88-9-1383](https://doi.org/10.1175/BAMS-88-9-1383)
- Meehl GA, Stocker TF, Collins WD, Friedlingstein P, Gaye AT, Gregory JM, Kitoh A, Knutti R, Murphy JM, Noda A, Raper SCB, Watterson IG, Weaver AJ, Zhao ZC (2007b) Global climate projections. In: Solomon S, Qin D, Manning M, Marquis M, Averyt K, Tignor MMB, Miller HL, Chen Z (eds) *Climate change 2007: the physical science basis. Contribution of working group I to the fourth assessment report of the intergovernmental panel on climate change*, Cambridge University Press, Cambridge, pp 747–845
- Oshima K, Tanimoto Y (2009) An evaluation of reproducibility of the Pacific decadal oscillation in the CMIP3 simulations. *J Meteorol Soc Jpn* 87:755–770. doi:[10.2151/jmsj.87.755](https://doi.org/10.2151/jmsj.87.755)
- Oshima K, Tanimoto Y, Xie SP (2012) Regional patterns of wintertime SLP change over the North Pacific and their uncertainty in CMIP3 multi-model projections. *J Meteorol Soc Jpn* 90:385–396. doi:[10.2151/jmsj.2012-A23](https://doi.org/10.2151/jmsj.2012-A23)
- Pardaens AK, Gregory JM, Lowe JA (2011) A model study of factors influencing projected changes in regional sea level over the twenty-first century. *Clim Dyn*. doi:[10.1007/s00382-009-0738-x](https://doi.org/10.1007/s00382-009-0738-x)
- Sakamoto TT, Hasumi H, Ishii M, Emori S, Suzuki T, Nishimura T, Sumi A (2005) Responses of the Kuroshio and the Kuroshio Extension to global warming in a high-resolution climate model. *Geophys Res Lett* 32(L14617). doi:[10.1029/2005GL023384](https://doi.org/10.1029/2005GL023384)
- Sato Y, Yukimoto S, Tsujino H, Ishizaki H, Noda A (2006) Response of North Pacific ocean circulation in a Kuroshio-resolving ocean model to an Arctic Oscillation (AO)-like change in Northern Hemisphere atmospheric circulation due to greenhouse-gas forcing. *J Meteorol Soc Jpn* 84:295–309
- Slangen ABA, Katsman CA, van de Wal RSW, Vermeersen LLA, Riva REM (2011) Towards regional projections of twenty-first century sea-level change based on IPCC SRES scenarios. *Clim Dyn*. doi:[10.1007/s00382-011-1057-6](https://doi.org/10.1007/s00382-011-1057-6)
- Sugimoto S, Hanawa K (2009) Decadal and interdecadal variations of the Aleutian Low activity and their relation to upper ocean variations over the North Pacific. *J Meteorol Soc Jpn* 87:601–614. doi:[10.2151/jmsj.87.601](https://doi.org/10.2151/jmsj.87.601)
- Suzuki T, Hasumi H, Sakamoto TT, Nishimura T, Abe-Ouchi A, Segawa T, Okada N, Oka A, Emori S (2005) Projection of future sea level and its variability in a high-resolution climate model: ocean processes and Greenland and Antarctic ice-melt contribution. *Geophys Res Lett* 32(L19706). doi:[10.1029/2005GL023677](https://doi.org/10.1029/2005GL023677)
- Suzuki T, Ishii M (2011) Regional distribution of sea level changes resulting from enhanced greenhouse warming in the Model for Interdisciplinary Research on Climate version 3.2. *Geophys Res Lett* 38(L02601). doi:[10.1029/2010GL045693](https://doi.org/10.1029/2010GL045693)
- Sverdrup HU (1947) Wind-driven currents in a baroclinic ocean; with application to the equatorial currents of the Eastern Pacific. *Proc Natl Acad Sci U S A* 33:318–326
- Trenberth KE, Hurrell JW (1994) Decadal atmosphere–ocean variations in the Pacific. *Clim Dyn* 9:303–319
- Uppala SM et al (2005) The ERA-40 reanalysis. *Q J R Meteorol Soc* 131:2961–3012. doi:[10.1256/qj.04.176](https://doi.org/10.1256/qj.04.176)
- Yamaguchi K, Noda A (2006) Global warming patterns over the North Pacific: ENSO versus AO. *J Meteorol Soc Jpn* 84:221–241
- Yin J, Griffies SM, Stouffer RJ (2010) Spatial variability of sea level rise in twenty-first century projections. *J Clim* 23:4585–4607. doi:[10.1175/2010JCLI3533.1](https://doi.org/10.1175/2010JCLI3533.1)